

Propagation effects of bichromatic laser pulses on the induced terahertz-radiation generation in a gaseous medium

Xiaofang Shu ¹, Zhifang Feng,² Chengxin Yu ^{3,*} and Jie Liu⁴

¹*Beijing Academy of Quantum Information Sciences, Beijing, 100193, People's Republic of China*

²*College of Applied Science, Taiyuan University of Science and Technology, Taiyuan 030024, People's Republic of China*

³*Institute of Applied Physics and Computational Mathematics, Beijing 100088, People's Republic of China*

⁴*Graduate School of China Academy of Engineering Physics, Beijing, 100193, People's Republic of China*



(Received 10 June 2022; accepted 4 October 2022; published 20 October 2022)

In this work, a simplified propagation model is proposed to specifically study the propagation effects of the driving laser pulse on the terahertz radiation in a gaseous medium for a short propagation distance. The simulations indicate that, due to the atomic ionization process and the energy redistribution between the laser field and the ionized electrons, the bichromatic laser pulses experience significant energy decaying, blue-shift, and a trailing edge broadening. As a result, the behaviors of the ionized electrons in the deformed laser field lead to the blue-shift and the multipeak structures in the terahertz radiation spectrum. Further investigations show that the differences of the terahertz spectrum for different relative phases of the fundamental and the second harmonic fields are gradually fading away as the driving laser pulse propagates. All these results strongly suggest that the propagation effects should be taken into consideration while it is generally disregarded.

DOI: [10.1103/PhysRevA.106.043514](https://doi.org/10.1103/PhysRevA.106.043514)

I. INTRODUCTION

In the past decades, the terahertz (THz) radiation that lies between the microwave and the infrared regions of the electromagnetic spectrum attracted extensive interests for its increasing potential in areas of research, industry, and defense [1–4]. For example, the THz radiation can penetrate fabrics as well as other materials, which allows it to image and detect concealed threats such as weapons, explosives, or chemicals in security areas [4–9]. The THz band also opens a rich spectral window for numerous low-energy excitation, such as vibrations of the crystal lattice, rotations of molecules, spin waves, internal excitation of electron-hole pairs, phonons in crystalline solids, and the hydration states of a biological system [10–12].

One of the main THz generation mechanisms is the optical rectification model in which the fundamental frequency of an infrared femtosecond laser pulse was down-converted to THz regime via second-order susceptibility in noncentrosymmetric crystals. Another crucial mechanism is the transient current model, where the photoconductive current driven by external electromagnetic fields in solid or gaseous media plays an important role. For instance, the produced plasma by the gaseous or solid media subjected to the strong laser fields acts as frequency converter towards the THz range [13–16]. The superposed asymmetric optical field makes the ionized electrons drift to produce a directional net current in the low-frequency regime, which emits the THz radiation obeying the Jefimenkos' equation [17]. Microscopically, the generation of THz radiation originates from the motion of electrons, such

as the released electrons through the field-ionizing processes in the intense laser field and the photoconductive electrons in semiconductor medium excited by femtosecond lasers, and the spin-carrying electrons in two-dimensional semiconductors exposed to magnetic fields, and so on.

Since there is no damage threshold for gaseous media, air or noble gases are usually used as the source for generating THz radiation [18,19]. By adjusting the incident laser parameters, such as frequencies and relative phase differences, one can obtain the terahertz radiations that meet various corresponding needs. In these situations, the ultimate goal is to control the trajectories and velocities of electrons in the external fields [20–27].

During the generation of the THz radiation, the driving laser pulses inevitably travel a certain distance in the gaseous medium in which the profile of the laser pulses would experience attenuation and deformation and so on due to the field-ionizing process, and all of these effects need to be taken into account (see the schematic diagram in Fig. 1). Though extensive research on the generation of terahertz radiation as the intense laser pulse propagates a meter-scale distance in air have been done, only the propagation of the envelope of the laser pulse is considered. While the short-range propagation of the entire temporal profile of the laser field in inert gases was extensively studied in the generation of high-order harmonics, it is not the case for THz radiation. It is to be expected that the THz radiation would undergo complicated changes in both frequency and temporal domains.

In this paper, we propose a simplified model for the propagation of driving laser pulse based on the Maxwell equations and the field ionization model and then investigate the generation of THz radiation. We choose a linearly polarized and synthesized laser pulse consisting of a fundamental

*cx_yu2013@163.com

frequency field and its second harmonic field, where the relative phase is an adjustable parameter. The strength of the laser fields lies in the tunneling ionization regime and the mechanism of the THz radiation generation is the transient current. Throughout this paper, the international system of units is adopted unless otherwise noted.

II. THEORETICAL MODEL

As an intense laser pulse propagates in a gaseous medium, its temporal evolution is governed by the Maxwell equations coupled with field-ionized models, such as tunnel ionization, multiphoton ionization, and so on. To reduce the computational costs, it is convenient to adopt the comoving frame, $\tau = t - z/c$ and $\xi = z$, where t and z are the time and propagation variables in the laboratory frame and c is the speed of light in a vacuum. By using the slow-varying envelop approximation ($|\frac{\partial^2}{\partial \xi^2}| \ll |k_0 \frac{\partial}{\partial \xi}|$ with the wave number k_0), the propagation equation reads [28,29]

$$-\frac{2}{c} \frac{\partial^2 \mathbf{E}}{\partial \xi \partial \tau} + \nabla_{\perp}^2 \mathbf{E} = \mu_0 \frac{\partial^2 \mathbf{P}_i}{\partial \tau^2} + \mu_0 \frac{\partial \mathbf{J}_e}{\partial \tau}, \quad (1)$$

where $\nabla_{\perp}^2 = \partial^2/\partial x^2 + \partial^2/\partial y^2$ is the transverse Laplace operator that contributes to the diffraction of the laser beams. When the propagation distance (~ 1 cm) is far less than the Rayleigh length, the transverse diffraction effects can be neglected. In addition, for a dilute gaseous medium, the contribution to the electric polarization from the neutral atoms is not taken into consideration because it is sufficiently small compared with that from the ionized electrons [28]. The electric polarization response $\mathbf{P}_i(\tau)$ characterizes the atomic ionization process, $\mathbf{J}_e(\tau)$ is the electric current caused by the ionized electrons in the laser field, and μ_0 is the permeability of the vacuum.

During the atomic ionization of the gaseous medium, the energy loss rate can be evaluated by $\mathbf{E}(\tau)d\mathbf{P}_i(\tau) = eI_p d\rho_e(\tau)$, which gives

$$\frac{\partial \mathbf{P}_i(\tau)}{\partial \tau} = eI_p \frac{\mathbf{E}(\tau)}{|E(\tau)|^2} \frac{\partial \rho_e}{\partial \tau}. \quad (2)$$

Here, I_p is the atomic ionization potential and e is the electron charge. The time-dependent electron density ρ_e is described by the rate equation

$$\frac{\partial \rho_e(\tau)}{\partial \tau} = W(\tau)[\rho_0 - \rho_e(\tau)], \quad (3)$$

where ρ_0 is the initial density of the neutral atoms and $W(\tau)$ is the ionization rate. In this work, we adopt the Ammosov-Delone-Krainov (ADK) model [30] to obtain the value of $W(\tau)$ without loss of generality.

The plasma current $\mathbf{J}_e(\tau)$ is caused by the movement of the ionized electrons in the laser field and it depends on the transient velocity and the electron density

$$\mathbf{J}_e(\tau) = e \int_{-\infty}^{\tau} \frac{\partial \rho_e}{\partial \tau'} \mathbf{V}(\tau, \tau') d\tau', \quad (4)$$

where $\mathbf{V}(\tau, \tau')$ is the velocity at τ of the ionized electron with the birth time τ' .

By integrating Eq. (1) over the time $[-\infty, \tau]$ from both sides and using Eqs. (2) and (4), the propagation equation of

the intense laser pulses can be written in integral-differential form as [28]

$$\frac{\partial \mathbf{E}(\tau)}{\partial \xi} = -\frac{e\mu_0 c I_p}{2} \left[\frac{\mathbf{E}(\tau)}{|E(\tau)|^2} \frac{\partial \rho_e}{\partial \tau} \right] - \frac{1}{2c} \int_{-\infty}^{\tau} \omega_p^2(\tau') \mathbf{E}(\tau') d\tau', \quad (5)$$

where $\partial \mathbf{V}(\tau, \tau')/\partial \tau = e\mathbf{E}(\tau)/m_e$ is used, the time-dependent plasma frequency $\omega_p(\tau) = \sqrt{\rho_e(\tau)e^2/(m_e \epsilon_0)}$, $\mu_0 \epsilon_0 = 1/c^2$, and m_e is the rest mass of an electron. The first term on the right-hand side represents the laser energy loss due to the optical field-ionization of the gaseous medium. The second term means that the ionized electrons gain their kinetic energies from the laser field and then oscillate with the time-varying frequency $\omega_p(\tau)$. For convenience, we ignore the explicit dependence of physical quantities to ξ .

According to the Jefimenkos' theory [17], the far-field THz radiation is proportional to the derivative of the electric current with respect to τ , $\mathbf{E}_{\text{THz}}(\tau) \propto \partial \mathbf{J}_e(\tau)/\partial \tau$. From Eq. (4), we have

$$\frac{\partial \mathbf{J}_e(\tau)}{\partial \tau} = \epsilon_0 \omega_p^2(\tau) \mathbf{E}(\tau). \quad (6)$$

The radiation field and the corresponding power spectrum of THz are calculated as

$$\begin{aligned} \tilde{\mathbf{E}}_{\text{THz}}(\Omega) &\propto \int_{-\infty}^{+\infty} \frac{\partial \mathbf{J}_e(\tau)}{\partial \tau} \exp(-i\Omega\tau) d\tau \\ &= \epsilon_0 \tilde{\omega}_p^2(\Omega) * \tilde{\mathbf{E}}(\Omega), \end{aligned} \quad (7)$$

$$P_{\text{THz}}(\Omega) \propto |\tilde{\mathbf{E}}_{\text{THz}}(\Omega)|^2, \quad (8)$$

where the symbol “*” in the second line of Eq. (7) means the convolution operation in the frequency domain.

III. SIMULATIONS AND DISCUSSIONS

In this work, the linearly polarized two-color laser pulses consisting of a leading pulse with the central wavelength $\lambda_L = 800$ nm and its second harmonic field (400 nm) are used,

$$E_{\text{in}}(\tau) = E_0 f(\tau) [\cos(\omega_L \tau) + \zeta \cos(2\omega_L \tau + \phi)], \quad (9)$$

where the surrounding $f(\tau) = \exp(-\tau^2/\tau_f^2)$ with $\tau_f = 40$ fs and the angular frequency $\omega_L = 2\pi c/\lambda_L$. The relative phase ϕ is an adjustable parameter. The electric strength E_0 relates to the peak intensity $I_0 = \epsilon_0 c E_0^2/2$. In this paper, the peak laser intensity of the fundamental frequency field is $I_0 = 2.0 \times 10^{14}$ W/cm², which corresponds to the tunneling ionization regime for the argon atom and the parameter $\zeta = \sqrt{0.1}$ represents the relative peak strength of the second-harmonic field. Considering the spreading of the laser pulse in the time domain during the propagation and the generation of THz radiation, the time domain that is considered in our computation ranges from -80 to 250 fs. The number of grid points for τ is 2^{14} , which corresponds to the time interval $\Delta\tau \approx 0.02$ fs. The laser pulse propagates for a distance of 1.0 cm and the fixed step size $\Delta\xi = 0.5$ μm .

The gas pressure of the dilute argon medium is set to be $p = 150$ Torr and the room temperature $T = 300$ K. Using the ideal gas-state equation, we obtain the initial density of the

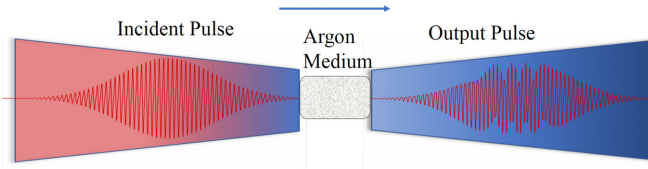


FIG. 1. The schematic diagram for the propagation of a laser pulse in gaseous medium.

neutral atoms as $\rho_0 = pT_{\text{std}}\rho_{\text{std}}/(p_{\text{std}}T) \approx 4.8 \times 10^{18} \text{ cm}^{-3}$, where $T_{\text{std}} = 273.15 \text{ K}$ and $p_{\text{std}} = 760 \text{ Torr}$ are the standard temperature and pressure, respectively. The density of particles in the standard condition is $\rho_{\text{std}} \approx N_A/(22.4 \times 10^3 \text{ cm}^3)$ with the Avogadro constant $N_A = 6.022 \times 10^{23}$.

In Figs. 2(a) to 2(d), we present the profiles of the electric pulse normalized by the incident peak electric strength E_m at four different propagation distances, where $E_m = \text{MAX}[E_{\text{in}}(\tau)] = 4.46 \times 10^{10} \text{ V/m}$, and the relative phase is $\phi = \pi/2$. For the sake of comparison, the incident laser pulse is also plotted by the black, dashed line. The overlaps (namely, before -20 fs) suggest that the laser pulse remains unchanged during the propagation in the early stage and the subsequent differences tell when and how the laser pulses change afterwards. Because the trailing parts of the laser pulses are quite

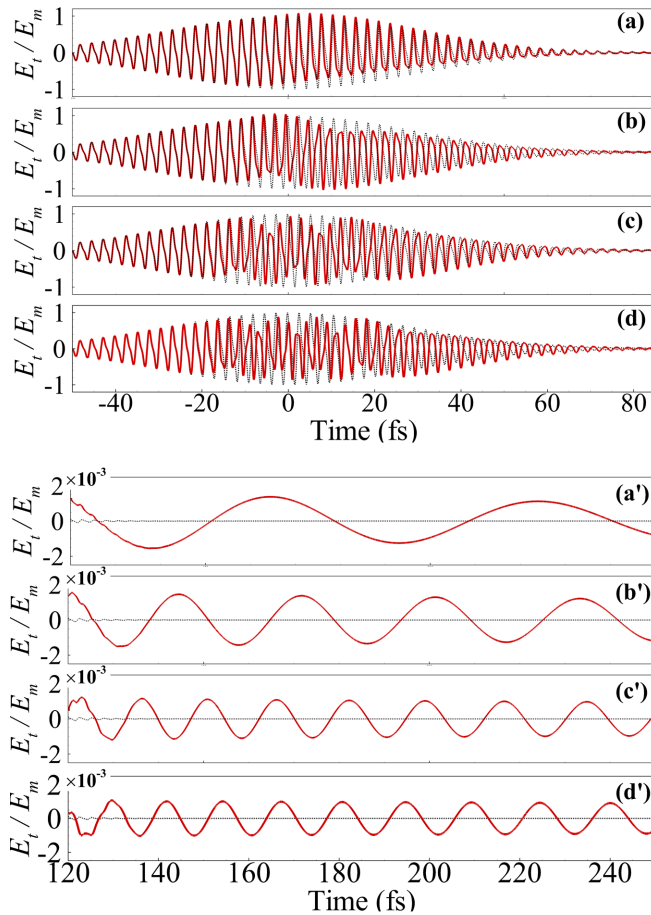


FIG. 2. The profile of the normalized output electric field by the incident peak electric strength E_m at different distances. (a,a') $\xi = 0.025 \text{ cm}$; (b,b') $\xi = 0.1 \text{ cm}$; (c,c') $\xi = 0.5 \text{ cm}$; (d,d') $\xi = 1 \text{ cm}$.

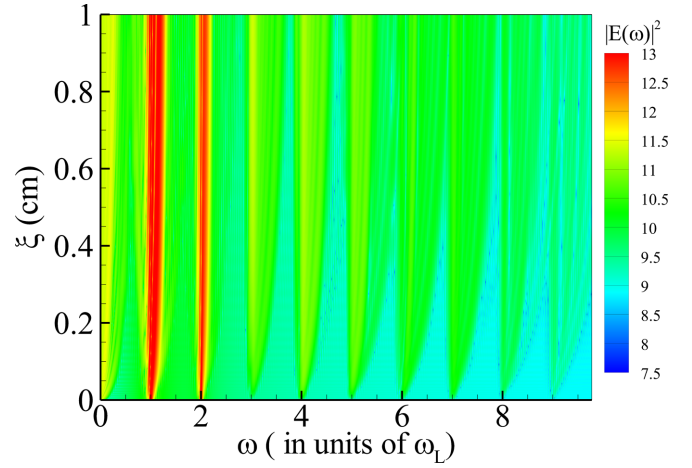


FIG. 3. The spectrum intensity of laser field in logarithmic scale during its propagation in the argon medium, where the abscissa is the normalized frequencies by the central frequency (ω_L) of the fundamental field.

long, and its strengths are relatively low, to make it easier to tell the differences, we zoom in the trailing parts of Figs. 2(a) to 2(d) as Figs. 2(a') to 2(d'), respectively. It can be clearly found that, in the time domain of -20 – 20 fs , the electric field experiences decaying and deforming as it propagates in the gaseous medium. In addition, the laser field is also obviously compressed in the temporal direction, which means the blue-shift in the frequency domain and the trailing edge of the pulse can also be observed to spread as a long tail and oscillates periodically.

In the tunneling ionization regime, the Keldysh parameter $\gamma_K = \omega_L \sqrt{2m_e I_p} / (eE) < 1$, which gives a critical electric field $E_c = \omega_L \sqrt{2m_e I_p} / e = 3.12 \times 10^{10} \text{ V/m}$ for the argon atom ($I_p = 15.7 \text{ eV}$) and the fundamental frequency field. It means that the electrons are freed rapidly when $|E_t/E_m| > E_c/E_m \approx 0.7$. It also means that the argon atoms begin to be ionized at about -20 fs and the electric field loses its energy during the ionization processes and then continues to exchange its energy with the ionized electrons. The second term on the right-hand side of Eq. (5) characterizes the motion of the ionized electrons in the laser field and it is a source term in the form of ω_p^2 -weighted cumulative integral with respect to τ , which causes the deformation and blue-shift of the laser pulse. For a given propagation distance, the density of the ionized electrons keeps almost unchanged for a sufficiently large time, such as $\tau > 80 \text{ fs}$, where the Keldysh parameter $\gamma_K \gg 1$. This means the plasma frequency $\omega_p(\tau)$ is also independent of the time when $\tau > 80 \text{ fs}$. Therefore, the source term is proportional to the simple integral of electric field $\mathbf{E}(\tau)$ at the trailing edge of the pulse. As the laser pulse propagates in the gaseous medium, the continuous accumulation of this source term results in the oscillations of the trailing edge with lower frequencies, as shown in Figs. 2(a') to 2(d').

The evolution of the spectrum of the laser pulse propagating in a medium is given in Fig. 3, where the abscissa is the frequencies normalized with respect to the central frequency (ω_L) of the fundamental field and the ordinate is the propagation distance. At the early stage of the laser propagation,

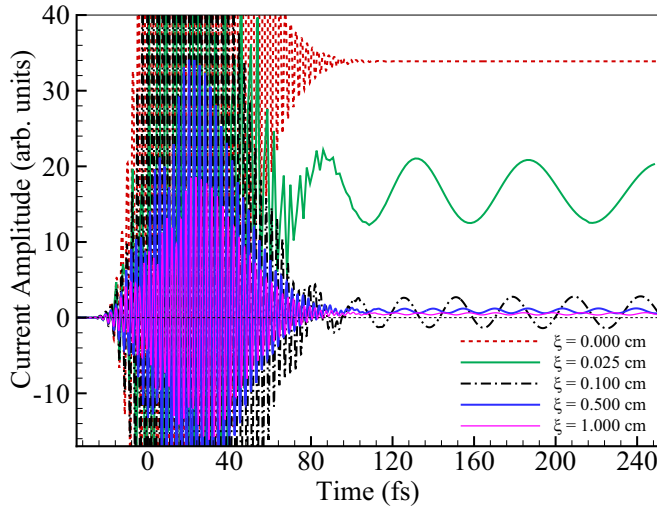


FIG. 4. The transient electric current of ionized electrons driven by the laser field at several typical propagation distances.

harmonics are observed due to extremely nonlinear interactions of the intense laser field and the gaseous atomic medium, such as atomic ionization, accelerations of ionized electrons whose density is time dependent. With the propagation of the laser field in the medium, blue-shift is observed in the fundamental field and all of its harmonics. In addition, the higher the harmonic order, the larger the magnitude of the blue shift. Notably, some components with lower frequencies that correspond to the long trailing edge of the laser pulse are also observed and they all shift to the blue band as the laser propagates in the medium. Since the incident laser field is initially bichromatic, the fundamental and second harmonic fields ($\zeta = \sqrt{0.1}$) are the leading parts during the propagation.

Using Eq. (6), we calculate the transient electric current for several different propagation distances, as shown by the lines with different colors and styles in Fig. 4. As discussed above, the ionized electrons are significantly generated after about -20 fs, the transient electric currents for different distances also start to appear at this moment. The red and dashed curve represents the initial electric current, and it has an obvious shift and has no oscillation because of the near-zero electric strength. The transient current denoted by the green, solid line is obtained for the propagation distance $\xi = 0.025$ cm and its values at the tail are reduced and have a period of about 55 fs. The periodicity of the transient current originates from that of the electric field and has almost the same period, see Fig. 2 (a'). When the distance $\xi = 0.1$ cm, the period of the values of the transient current at the back edge becomes smaller (~ 25 fs), see the black, dashed-dotted line in Fig. 4. The solid lines with blue and magenta colors are the results calculated for the distances of $\xi = 0.5$ cm and 1.0 cm, respectively, and the periods are both about 12 fs. Also, it is worth noting that the magnitude of the drift current which is obtained by Eq. (4) does not decrease monotonically during the laser propagation because the drift current depends on the temporal profile of the laser pulse for the given propagation distance.

According to Eqs. (7) and (8), the radiation spectrum is obtained by the convolution of the square of the plasma

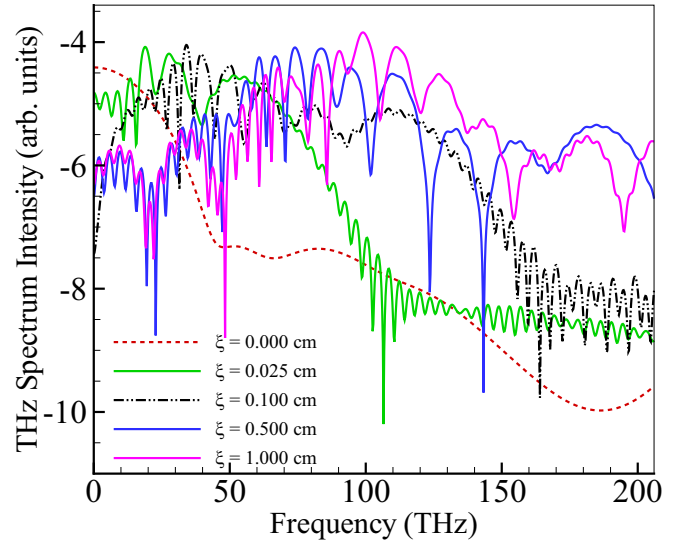


FIG. 5. The spectra intensity of terahertz radiation in logarithmic scale at the same propagation distances as in Fig. 4.

oscillation frequency and the strength of the laser field. To calculate the spectrum of the THz radiation, we choose the frequency window $\Omega \in [1, 250]$ THz and obtain the spectrum of the THz radiation, as shown in logarithmic scale in Fig. 5, where the relative phase is $\phi = \pi/2$. For the incident two-color laser pulse, the spectrum of terahertz radiation is given in red, dashed line. Evidently, there is a continuous spectrum with the maximal amplitude in the range of 0–10 THz. As the laser pulse propagates in the medium, due to the blue-shift and the broadening of the laser spectrum, the terahertz band also shifts to the blue edge. The case when $\xi = 0.025$ cm is given by the green, solid line. We can see that the range of the maximal magnitude in the terahertz spectrum blue-shifts to around $\Omega = 20$ –30 THz, where the multippeak structure also appears. The periodic oscillations of the transient current on the tail at this propagation distance have contributions to the spectrum of the terahertz radiation. The black, dashed-dotted line represents the terahertz spectrum with multiple peaks at $\xi = 0.1$ cm and the main peak blue-shifts to around $\Omega = 40$ THz. The region of lower frequencies is greatly suppressed, which corresponds to the low averaged current drift, see the tail of the black, dashed-dotted line in Fig. 4. In Fig. 5, The solid lines in blue and magenta colors are the terahertz radiation spectra at $\xi = 0.5$ cm and 1.0 cm, respectively. From Fig. 4, the average values of the current drift and the oscillation periods for these two distances differ very little on the tails between 120 and 250 fs, which means their low-frequency region (< 40 THz) almost coincide. The leading peaks blue-shift to around $\Omega = 80$ THz and $\Omega = 100$ THz, respectively.

To demonstrate the analysis above, we perform the same calculations for different relative phases between the fundamental field and its second harmonic field. In Fig. 6(a), we present the terahertz radiation spectrum produced by the initial laser field for different relative phases and the green, dashed line denotes the results from the phase $\phi = \pi/2$. Obviously the optimal terahertz radiation can be obtained when the relative phase $\phi = 0.45\pi$. As the laser pulse propagates

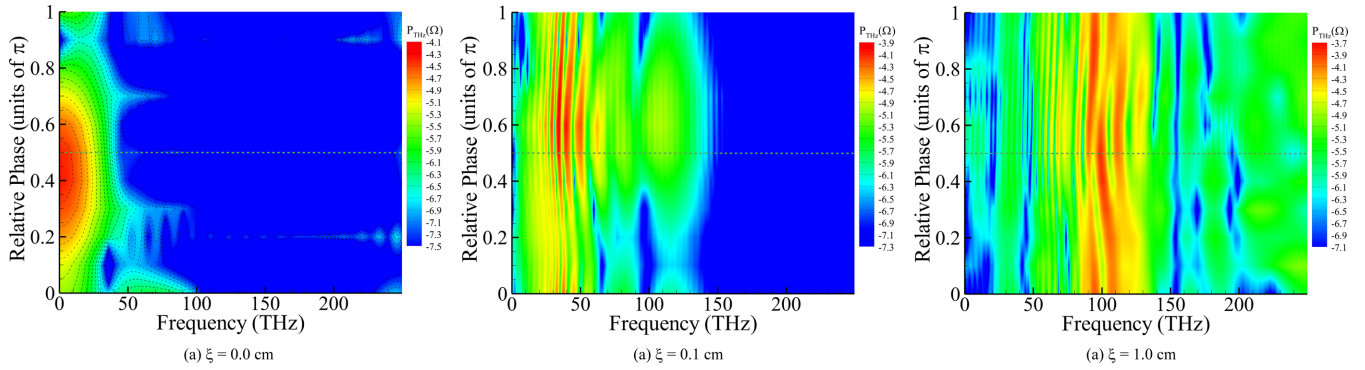


FIG. 6. The spectra of terahertz radiation for different relative phases at three typical propagation distances, where the color bars are in logarithmic scale and the ordinates are the relative phase ϕ .

for a distance of $\xi = 0.1$ cm, the spectrum of terahertz radiation is given in Fig. 6(b). We can obviously observe that the spectra have significant blue-shifts for all relative phases and the multipeak structures appear. The leading peaks of the terahertz radiation are round 30–50 THz, and the optimal relative phase is $\phi = 0.6\pi$ for such a distance. According to the classical electromagnetic theory, the spectral structures of terahertz radiation originate from the ionization process of electrons and their complicated motions in the deformed laser electric field. When the propagation distance is 1.0 cm, the spectra of terahertz radiation are further blue-shifted, the positions of the central frequencies are about $\Omega = 100$ THz, and the difference in the radiation spectrum becomes smaller for different relative phases.

The simulations for different relative phases demonstrate that the interaction between strong laser field and atomic medium leads to the blue-shift and multipeak structures of the terahertz radiation spectrum during the laser propagation. The ionized electrons redistribute the laser energy in the temporal domain, which causes the deformation and compression of the laser profile. Compared with the cases for different relative phases, the leading peaks of the terahertz radiation spectra are all blue-shifted to around 100 THz after the laser pulse propagates for a distance of $\xi = 1.0$ cm and the optimal relative phases for the terahertz radiation spectra at the lower frequencies ($0 \sim 10$ THz) are $0.5\pi \sim 0.6\pi$ and around 0.8π . All the THz spectrum differences caused by different relative phases are gradually smoothed out due to the spectral broadening of the laser field.

IV. CONCLUSION

In summary, we propose a simplified model for the propagation of the intense laser pulse, which is specifically used to investigate the propagation effects of the two-color laser pulse on the THz radiation in an argon medium. The terahertz radiation mechanism used above is the transient photocurrent mechanism and using the Jefimenkos' theory we analyze the terahertz radiation induced by the plasma current of the ionized electron in the laser field.

In deriving the propagation equation of the laser pulse in a gaseous argon medium, we adopt the comoving frame and slowly varying envelope approximation. The reason why the

gas is said to be dilute in our model is that some effects of the neutral atoms on the laser can be ignored compared to the effects of the ionized electrons, such as nonlinear Kerr effects, refraction effects since the refraction index $n \sim 1$, and so on. In addition, we also drop the lateral diffraction effects due to the short propagation distance.

The simulations indicate that the intense incident laser field causes significant tunneling ionization of gaseous atoms, which leads to the time-varying densities of medium constituents. The atoms first absorb sufficient energies from the laser field to release their electrons and then the ionized electrons are accelerated by the laser electric field. In the propagation equation, the acceleration process is weighted by the density of the ionized electrons and contributes to the evolution of the laser pulse as a source term. Consequently, the complicated behaviors of the ionized electrons leads to the deformation of the laser pulse with the decay of the strength and the spectral blue-shift. It is found that the terahertz radiation undergoes a considerable blue shift and a multipeak structure appears. Furthermore, the contributions to the terahertz radiation mainly come from the net drift of the current and the oscillation of the current tail, and discrepancies from the different initial relative phases are smoothed out gradually. Therefore, we come to the conclusion that the propagation effects should be considered in the study of the THz radiation caused by the interaction of an intense femtosecond laser pulse with gaseous medium.

It is notable that, in this work, we only consider the dilute gaseous medium in which the effects of the neutral atoms and Kerr nonlinearity are neglected. The diffraction of the laser beam is also not taken into consideration because of the short propagation distance. When the density of the applied medium is sufficiently high, or the propagation distance is quite long enough, all the dropped terms in the propagation equation (1) should be reevaluated.

ACKNOWLEDGMENTS

The authors are grateful for financial support from the National Natural Science Foundation of China (Grants No. 12004043, No. 11775030, and No. 11875091) and the National Key Research and Development Program (Grant No. 2018YFB0504400).

- [1] X.-C. Zhang and J. Z. Xu, *Introduction to THz Wave Photonics* (Springer, Boston, 2010).
- [2] P. H. Siegel, *IEEE Trans. Microwave Theory Tech.* **50**, 910 (2002).
- [3] P. M. Solyankin, I. A. Nicolaeva, A. A. Angeluts *et al.*, *New J. Phys.* **22**, 013039 (2020).
- [4] M. Tonouchi, *Nat. Photonics* **1**, 97 (2007).
- [5] P. Y. Han and X.-C. Zhang, *Meas. Sci. Technol.* **12**, 1747 (2001).
- [6] L. Ho, M. Pepper, and P. Taday, *Nat. Photonics* **2**, 541 (2008).
- [7] B. Fischer, M. Hoffmann, H. Helm, G. Modjesch, and P. Jepsen, *Semicond. Sci. Technol.* **20**, S246 (2005).
- [8] I. Duling and D. Zimdars, *Nat. Photonics* **3**, 630 (2009).
- [9] K. Ahi and M. Anwar, *Proc. SPIE* **9856**, 98560G (2016).
- [10] T. L. Cocker and R. Huber, *Nat. Photonics* **7**, 678 (2013).
- [11] T. Kampfrath, K. Tanaka, and K. A. Nelson, *Nat. Photonics* **7**, 680 (2013).
- [12] B. Zaks, R. B. Liu, and M. S. Sherwin, *Nature (London)* **483**, 580 (2012).
- [13] X. Xie, J. M. Dai, and X.-C. Zhang, *Phys. Rev. Lett.* **96**, 075005 (2006).
- [14] A. Stathopoulos, S. Skupin, and L. Bergé, *Opt. Lett.* **46**, 5906 (2021).
- [15] Y. Q. Song, M. X. Yuan, G. Q. Lin *et al.*, *Opt. Express* **29**, 433379 (2021).
- [16] S. J. Liu, Z. Q. Fan, C. H. Lu, J. Y. Gui, C. Luo, S. X. Wang, Q. Q. Liang, B. Zhou, A. Houard, A. Mysyrowicz, V. Kostin, and Y. Liu, *Phys. Rev. A* **102**, 063522 (2020).
- [17] O. Jefimenko, *Electricity and Magnetism: An Introduction to the Theory of Electric and Magnetic Fields* (Electret Scientific, Star City, WV, 1989).
- [18] Z. Zhang, Y. Chen, M. Chen, Z. Zhang, J. Yu, Z. Sheng, and J. Zhang, *Phys. Rev. Lett.* **117**, 243901 (2016).
- [19] Q. Song, Q. Lin, H. Wang, H. Zhong, Y. Cai, S. Zheng, Z. Chen, X. Lu, X. Zeng, H. Shangguan, H. Wang, and S. Xu, *Phys. Rev. A* **102**, 023506 (2020).
- [20] H. Xiao, S. Wang, Y. Peng, D. M. Mittleman, J. Zhao, Z. Jin, Y. Zhu, and S. Zhuang, *Phys. Rev. A* **104**, 013517 (2021).
- [21] T. Löffler, F. Jacob, and H. G. Roskos, *Appl. Phys. Lett.* **77**, 453 (2000).
- [22] A. Houard, Y. Liu, B. Prade, V. T. Tikhonchuk, and A. Mysyrowicz, *Phys. Rev. Lett.* **100**, 255006 (2008).
- [23] J. Dai, N. Karpowicz, and X.-C. Zhang, *Phys. Rev. Lett.* **103**, 023001 (2009).
- [24] H. D. Wen and A. M. Lindenberg, *Phys. Rev. Lett.* **103**, 023902 (2009).
- [25] X. F. Shu, C. X. Yu, and J. Liu, *Phys. Plasmas* **26**, 023108 (2019).
- [26] H. G. Wang, N. Li, Y. Bai, P. Liu, Z. S. Wang, and C. P. Liu, *Opt. Express* **25**, 30987 (2017).
- [27] K. Y. Kim, J. H. Glowina, A. J. Taylor, and G. Rodriguez, *Opt. Express* **15**, 4577 (2007).
- [28] C. X. Yu and J. Liu, *Phys. Rev. A* **90**, 043834 (2014).
- [29] X. F. Shu, C. X. Yu, and J. Liu, *Appl. Phys. B* **125**, 35 (2019).
- [30] M. V. Ammosov, N. B. Delone, and V. P. Krainov, *Zh. Eksp. Teor. Fiz.* **91**, 2008 (1986) [*Sov. Phys. JETP* **64**, 1191 (1986)].